Journal of
Nanomedicine & Nanotechnology

Shinde et al. J Nanomedic Nanotechnol 2015, S7
DOI: 10.4172/2157-7439.S7-004

Research Article Open Access

Time Dependent Facile Hydrothermal Synthesis of TiO_2 Nanorods and their Photoelectrochemical Applications

Shinde DB[1], Jagadale SK[1], Mane RK[2]*, Mane RM[1], Ghanwat VB[1], Khot KV[1], Mali SS[3], Hong CK[3] and Bhosale PN[1]*

[1]*Materials Research Laboratory, Department of Chemistry, Shivaji University, Kolhapur 416004, India*
[2]*Department of Chemistry, Shivaji University, Kanya Mahavidyalaya, Islampur, Sangali, India*
[3]*Polymer Energy Materials Laboratory, Advanced Chemical Engineering Department, Chonnam National University, Gwangju, South Korea*

Abstract

In the present investigation, we report facile hydrothermal synthesis of TiO_2 nanorods with high density rutile phase on Transparent Conducting Oxide (TCO) for enhanced solar cell application. The structural, optical, morphological, compositional and electrochemical properties are investigated by detailed XRD, UV-Vis-NIR spectrophotometer, FESEM, TEM, EDAX, XPS and photoelectrochemical studies. It is demonstrated that, the deposited TiO_2 thin film shows pure rutile phase with tetragonal crystal structure. Optical spectra showed strong light absorption in UV region and FESEM images confirm the time dependent growth of TiO_2 nanorods. EDAX and XPS Spectra confirm the formation of pure TiO_2 nanorods. Photoelectrochemical performance with respect to time dependent growth of TiO_2 nanorods showed highest photoconversion efficiency η = 5.1%.

Keywords: Hydrothermal synthesis; TiO_2 nanorods; Transparent conducting oxide (TCO); Single crystalline; Photoelectrochemical cell property; Photoconversion efficiency

Introduction

Searching of alternative energy source is a vital issue in the modern civilization for many reasons which include depletion of conventional energy sources like coal, oil, natural gas etc. and burning of these energy fuels leading to a global air pollution problem. Hence there has been increasing interest during the last few decades to find out an alternative cost effective renewable energy sources to fulfill the future energy needs of mankind. In this respect synthesis of tailored morphological Transitional Metal Oxide (TMO) semiconducting thin films because of their widespread applications in optoelectronic fields of science and technology leading to drastic cut in the production cost of semiconducting devices. Exploring novel approaches to produce low cost, high efficiency photovoltaic cells has attracted attention of researchers because of the urgent need for the clean and renewable energy sources.

TiO_2 is a wide band gap (3.2 eV) transition metal oxide (TMO) semiconductor has received increasing attention due to its unique properties such as high chemical stability, high refractive index, optical transparency in UV and visible range, semiconducting behavior, photocatalytic activities, high PEC efficiency, biocompatibility, long term photostability, non-toxicity and low cost etc [1-5]. Because of all these properties TiO_2 become a common multifunctional material used in variety of applications in many fields such as dye sensitized solar cells [6], energy storage, gas sensors and biosensors [7], photocatalytic water splitting [8], photodegradation of organic pollutants, hydrogen generation [9,10], self-cleaning coatings [11], supercapacitors [12], electronic components [13], chemical catalysis [14], glass and ceramics [15], paintings, medicines, bactericides [16], cancer therapy [17] etc. Nanostructures of TiO_2 can exist in three crystal structures; two tetragonal forms (anatase and rutile) and one rhombic form (brookite). Among them the (110) surface of rutile TiO_2 has been shown to be highly active for photocatalytic water splitting and numerous other applications in photochemistry and catalysis [11,18]. In particular due to their higher surface to volume ratio, TiO_2 nanomaterials demonstrate high performance levels for these applications compared to their bulk form.

Number of methods have been reported to fabricate TiO_2 single crystal [19], nanorods, nanowires [20], tube arrays and nanospheres [21] that include template-assisted method [22], electrochemical anodic oxidation method [23], spray pyrolysis technique [24], chemical vapor deposition (CVD) [25], hydrothermal method [26], anodized aluminum oxide (AAO) template assisted sol-gel method [27], AAO template-assisted electrodeposition method [28], electrochemical anodic oxidation of pure titanium sheet [29], egg shell membrane template [30], electro-spinning [31] and chemical treatment of fine TiO_2 particles [32]. Among these diverse conventional methods, hydrothermal method is a simple and cost effective method for synthesis of well aligned nanostructures with easily obtained single-crystalline material having high specific surface areas [33]. It may provide a better opportunity for controlling the size and morphology of TiO_2 material for better photoconversion efficiency.

Various kinds of nanostructured TiO_2 such as nanoparticle, nanorods, nanotubes, hollow sphere, mesoporous and macroporous TiO_2 have been synthesized and used as a photoanode for the PEC application. Among this nanorod structured photoelectrodes are capable for improving the PEC performance due to their special 3D nanostructures [34]. It has been observed that for pure 1D nanorod arrays the unabsorbed light penetrates precisely through nanorods without being scattered for the enhancement of light absorption in the improvement of PEC performance [35]. Concerning the advantage of 3D nanorod flowers over 1D nanorods is not only multi reflection

***Corresponding author:** Bhosale PN, Materials Research Laboratory, Department of Chemistry, Shivaji University, Kolhapur-416004, (M.S), India, Tel: +91-231-2609338; Fax: +91-231-2691533; E-mail: p_n_bhosale@rediffmail.com

Mane RM, Department of Chemistry, Shivaji University, Kanya Mahavidyalaya, Islampur, Sangali, India, Tel: 9921482155; E-mail: rmane.1970@gmail.com

Received November 25, 2015; **Accepted** December 16, 2015; **Published** December 26, 2015

Citation: Shinde DB, Jagadale SK, Mane RK, Mane RM, Ghanwat VB, et al (2015) Time Dependent Facile Hydrothermal Synthesis of TiO_2 Nanorods and their Photoelectrochemical Applications. J Nanomedic Nanotechnol S7:004. doi:10.4172/2157-7439.S7-004

but also number of times scattering of incident light for better light harvesting and results in improvement in efficiency.

On the basis of above consideration, we have intent to develop a simple synthetic strategy to fabricate nanorod microstructure for the PEC cell performance. In this paper, we have demonstrated a time dependent hydrothermal evolution of TiO_2 nanorod microstructure with varying the reaction time from 2 h to 8 h. As the reaction time prolonged formation of nanorod flowers with increased diameter takes place. The nanorods are dense and uniformly covered the surface of the substrate. Such TiO_2 nanorods provide a large surface area and higher absorption of incident photons, which leads to more photogenerated electron-hole pair, causes higher PEC performance.

Method and Materials

Fluorine doped tin oxide (FTO) coated glass substrates with a sheet resistance of 25 Ωcm^{-2} used as a conducting substrate support for deposition of TiO_2 thin films. All chemical reagents used in this work were analytical reagent (AR) grade, and they were used without further purification. Titanium tetraisopropoxide (TTIP) (99.98% Spectrochem, India), hydrochloric acid (HCl) used as the Ti precursor. The aqueous solution was prepared using double distilled water. The substrates were washed with detergent and then cleaned in double distilled water and acetone separately in an ultrasonic bath.

Thin film synthesis

In a typical synthesis 0.5 ml titanium tetra isopropoxide (TTIP) was added in aqueous solution containing 30 ml 1:1 HCl and stirred vigorously for 30 min. to obtained clear and transparent solution. The resultant solution was added into teflon lined stainless steel autoclave. The conducting FTO glass substrate is immersed into autoclave solution inclined to the wall with conducting side facing up and the autoclave was sealed and placed in an oven at 160°C for 2 h followed by natural cooling to room temperature. The substrate was removed from autoclave, cooled at room temperature and rinsed thoroughly using double distilled water. Thus the obtained TiO_2 sample designated as T_1. Using the same procedure, in order to study the effect of reaction time on structure, morphology and PEC performance, the synthesis were carried out at different reaction time such as, 4 h, 6 h and 8 h and samples were designated as T_2, T_3 and T_4 respectively. Temperature and precursor concentration maintained constant throughout the series of hydrothermal experiments.

Characterizations

The deposited TiO_2 thin films were characterized for their optical, structural, morphological, compositional and PEC properties. The film thickness was measured with surface profiler (contact mode XP-1 Ambios Technology) having 1 Å resolution. The optical absorption spectra were recorded at room temperature using UV-Vis-NIR spectrophotometer (Shimadzu, UV-1800) in the wavelength range of 350-800 nm. The room temperature photoluminescence (RTPL) spectra of the thin films were recorded by using JASCO (Japan, FP-8300). The crystal structure was investigated by X-ray diffraction (XRD) (Rigaku, D/MAX Uitima Japan) using Cu Kα radiation (λ = 1.54 Å) in 2θ range 20° to 80°. Crystallographic characterization was done by using transmission electron microscopy (TEM), high resolution transmission electron microscopy (HRTEM) and corresponding selected area electron diffraction (SAED) pattern by using TECNAI F20 Philips, operating at an acceleration voltage 200 kV. The surface morphology of the thin film was analyzed with Field emission scanning electron microscope (FESEM). FESEM (Model Hitachi S4800, Japan) was employed for closer insight into the TiO_2 morphology. The elemental composition of the deposited thin film was determined by Energy dispersive X-ray spectroscopy analysis (EDS). The valence states of elements deposited on sample surface was studied by X-ray photoelectron spectroscopy (XPS; VG Multilab 2000, Thermo VG Scientific, UK). The PEC performance of TiO_2 thin films were measured in the dark and under UV illumination by forming simple two electrode system, with the deposited thin films as a working electrodes and graphite as a counter electrode in 0.1 M NaOH electrolyte.

Results and Discussion

Possible reaction and growth mechanism

The mechanism for the formation of well aligned rutile nanorods can be explained by considering the results of the present study and the literature survey. The FTO substrates were used for the growth of 3D nanostructures, because due to the lattice mismatch bare glass substrates have been unsuccessful for this purpose. The addition of aqueous HCl causes the hydrolysis of the inorganic moieties. HCl adjusted the pH value of the reaction solution and retard hydrolysis of the precursor in the presence of water at low temperatures and reduces the surface energy of the crystal plane side wall and promoting anisotropic growth in the (110) direction. Under acidic conditions, the transformation of Ti^{2+} from Ti^{4+} avoided and stabilizes the oxidation state of Ti^{4+}. The TiO_2 thin film deposition follows heterogeneous nucleation which was achieved by low degrees of supersaturation [36]. Initially the TTIP hydrolyzed to titanium hydroxide and alcohol in aqueous acid medium. Titanium hydroxide form a complex with water and the rate of complex formation is controlled in acidic medium. The chemical reactions involved in the formation of TiO_2 is as follows,

$$Ti(OR)_4 + 4H_2O \longrightarrow Ti(OH)_4 + 4ROH \text{ (hydrolysis)} \quad (1)$$

$$Ti(OH)_4 \longrightarrow TiO_2xH_2O + (2-x)\,H_2O \text{ (condensation)} \quad (2)$$

At high temperature and pressure condition hydrolysis rate was accelerated and deposited hydroxide dimerises on the surface of FTO coated glass substrates with internal proton transfer leads to corner-sharing octahedral chains (Ti_3O bridges) characteristics of the rutile structure. The Cl^- ions adsorbed at the (110) facets having higher density of Ti atoms.

Hence there would be an interaction between Ti atoms and n-donor base Cl^-. This facilitate the anisotropic growth along (110) facets and decreases the growth rate along (001) facets which leads to the formation of rutile phase TiO_2 nanorods instead of particles.

The nanorods are aggregated and connect with one root leading to formation of 3D nanorod flowers. With increasing the reaction time plenty of TiO_2xH_2O and large amount of nanorods were aggregated leading radial growth of nanorods. Further increase in the reaction time leads to increases the average diameter and length of nanorods and large number of nanoparticle aggregates on the top of nanorods ascribed to formation of blocking layers which decreases the PEC performance of the material.

Optical absorbance study

Figure 1 shows an optical absorption spectra of TiO_2 thin films hydrothermally grown at temperatures 160°C for different reaction times (2 to 8 h). Fundamental of absorption corresponds to electron excitation from the valence band to the conduction band using ultraviolet and visible radiation. The absorption coefficient (α) as a function of photon energy (hυ) can be expressed by the Tauc relation,

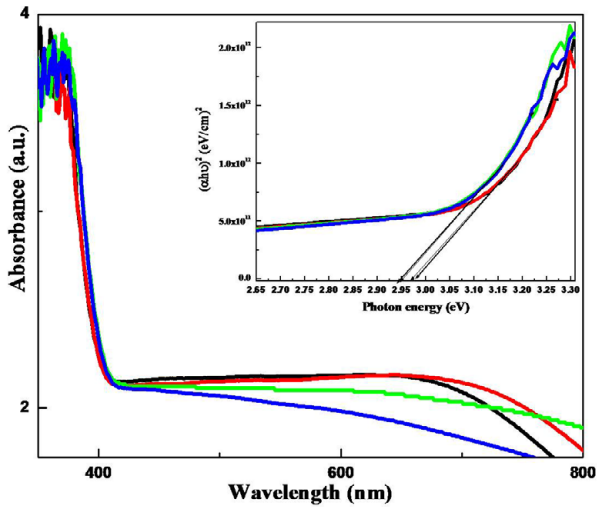

Figure 1: Shows an UV-Vis-NIR absorption spectra of TiO_2 thin films hydrothermally grown at temperatures 160°C for different reaction times, inset: shows plot of $(\alpha h\nu)^2$ vs. hν of the TiO_2 thin films.

$$\alpha h\upsilon = \alpha (h\upsilon - Eg)^n \quad (3)$$

where 'hυ' is photon energy, 'α' is constant, 'Eg' is band gap energy and 'n' is the exponential index determined by the nature of the electron transition during the absorption process. It is well known that there are fundamental optical transitions, namely direct allowed (n = 1/2) and indirect allowed (n = 2) transitions. Figure 1 inset shows plot of $(\alpha h\nu)^2$ vs. hν of the TiO_2 thin films. Extrapolating the straight line from the linear portion of the curve to the zero absorption edge gives the band-gap of the samples. The observed band gap energy of T_1-T_4 samples ranging from 2.93 to 2.97 eV respectively (Figure 1).

Photoluminescence study

Figure 2 Shows PL spectra of the T_1 to T_4 samples prepared by varying the reaction time and obtained over the wavelength range of 310-600 nm. The PL emission intensity can be related to the recombination dynamics of the excited electron and hole pairs. It is the emission of light, initiating from the recombination of photogenerated electron hole pairs. The PL spectrum of the TiO_2 nanostructures exhibits blue shift. All the samples possess the first intense peak at 322 nm assigned to direct transition of electron from conduction band to valance band. Higher the PL emission intensity, lower is the electron hole pair separation consequently lower the PEC performance. Therefore, the above observations can be understood the PL emission spectra of T_1 to T_4 samples at exciting wavelength of 325 nm. Among the entire samples, T_3 sample possess low PL intensity, suggesting longer life time for photogenerated charge carriers and higher PEC performance. Furthermore the other peaks appeared at longer wavelength 487, 450 and 409 nm corresponds to 2.51, 2.56 and 3.03 eV respectively can be attributed to the recombination that occurred at oxygen vacancies which are formed on the surface of TiO_2 due to crystal defects formed during hydrothermal synthesis and these defects act as the traps to cause luminescence [37] (Figure 2).

Structural study

The crystallite size and crystal structure of TiO_2 thin films was confirmed from the XRD analysis. Figure 4 shows XRD pattern of T_1-T_4 samples deposited at different reaction times. XRD patterns exhibited strong diffraction peaks at 27.55°, 36.79°and 55.40° indicating formation of rutile phase of TiO_2 material. The intense peak at 27.55^0 is the representative peak for (110) plane of rutile TiO_2 (Figure 3).

All other peaks observed at 36.79°, 39.12°, 41.42°, 44.29°, 55.40°, 62.72° and 64.29°, represents (101), (200), (111), (210), (220), (002) and (310) planes respectively which confirms the tetragonal crystal structure of TiO_2. The samples are well-crystallized in rutile TiO_2 single crystals, where the growth direction is along (001) orientation and the side surfaces exhibit (110) facets. All peaks are in good agreement with the standard JCPDS data (Card No. 00 001-0562) [38] and with the HRTEM and SAED results. The other peaks shown by asterisks are due to the FTO substrate marked by *. No other impurity peak in XRD pattern indicating no traces of secondary phases such as anatase or brookite were observed. The presence of broad XRD peaks is an indication of small crystallite size in the range of nanoscale, affirming the nanocrystalline nature of the TiO_2 samples. The rutile phase of TiO_2 is tetragonal and exhibits symmetry characters of the space group with two TiO_2 molecules per unit cell. Average crystallite size of TiO_2 samples were calculated by using Scherrer's formula shown in equation (4).

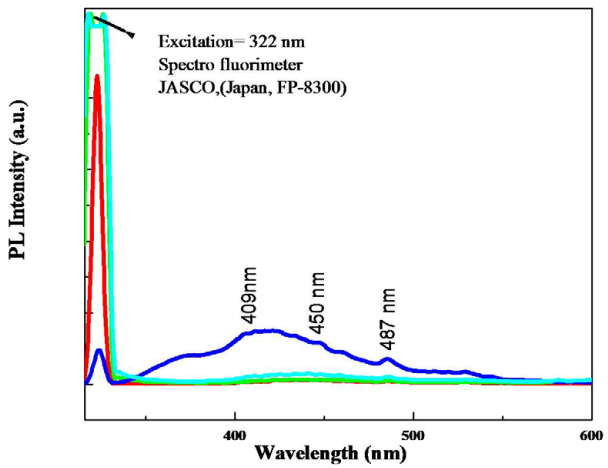

Figure 2: Shows photoluminescence (PL) spectra of theT_1 to T_4 samples prepared by varying the reaction time and obtained over the wavelength range of 350-600 nm.

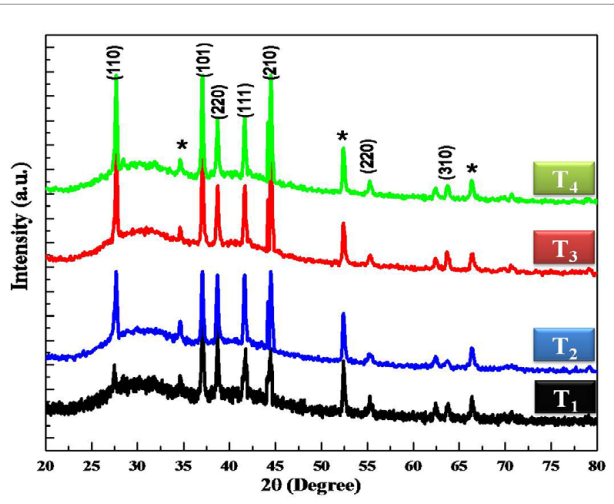

Figure 3: Shows XRD pattern of TiO_2 nanostructure samples (T_1–T_4) prepared by varying the reaction time.

$$D = \frac{0.94\lambda}{\beta \cos\theta} \quad (4)$$

Where 'D' is the crystallite size, 'θ' is peak position of X-ray used, 'β' is full width at half maxima (FWHM) of (110) plane of rutile TiO_2 and 'λ' is wavelength of X-ray used (0.154 nm). The increase in crystallinity size and intensity of reflections is observed with the increase in deposition time from 2 h to 8 h. The calculated crystallite size of TiO_2 for (110) planes are found to be 10, 16.13, 16.47 and 16.68 nm for T_1-T_4 samples respectively. The increase in crystallinity and intensity of reflections is observed with increase in deposition time.

To investigate the detailed structure and crystallinity of TiO_2 nanorods, TEM examination is performed. Figure 4a shows the TEM image focused on a single nanorod. A nanorod possesses 100 to 150 nm diameter and a tetragonal architecture with a smooth surface. The sharp SAED pattern shown in Figure 4b indicates that the nanorod is single crystalline. The Figure 4c shows the HRTEM pattern of TiO_2 nanorods. It indicates that the nanorods are completely crystalline along the entire lengths with the lattice spacing 0.344 nm, corresponding to the d-spacing of the (110) plane of rutile TiO_2. The predominant growth direction of (110) also agrees with the shape of crystal in rutile phase which is in good agreement with the XRD pattern (Figure 4a-4c).

Morphological study

Figure 5a-5d shows FESEM images of the TiO_2 thin films. During the hydrothermal reaction, the orientation, size, shape and morphology of the deposited material is mainly dependent on the reaction time, reaction temperature, precursors concentration, media and nature of substrate. In the present work a series of hydrothermal experiments with different reaction times were carried out to investigate the time-dependent morphological evolution of the TiO_2 thin films. We found that the formation of nanostructures was strongly dependent on the reaction time. As shown in Figure 5a, when the reaction time was as short as 2 h. nanorods were uniformly deposited on the substrate surface, (sample T_1). The lower reaction time results in the small growth of TiO_2 nanorods due to immature termination of growth process. When the reaction time was prolonged to 4 h the nanorods uniformly deposited to compact and large size 1D nanorod structure (Figure 5b). It is observed that the growth of nanorods on the surface of FTO substrate became larger and increased by about 30-40 nm per 2 h increase in reaction time. At the 4 h. reaction time (sample T_2) the nucleation process in the hydrothermal synthesis is fast which results in formation of well grown and well aligned nanorods. The FESEM image of the sample T_3 (Figure 5c) shows the compact arranged and well aligned nanorods. On the top surface of nanorods, aggregation of nanorod bunches connects with one root to form 3D nanorod flowers. Thus sample T_3 shows smooth, completely grown and regularly arranged nanorods with irregularly arranged nanorod flowers on their top surface. These irregularly arranged nanorods are smaller than the regularly arranged nanorods. Thus, at the reaction time 6 h (sample T_3) there is transformation from initially grown and orderly arranged nanorods to completely grown TiO_2 nanorods. There is formation of 3D nanorod flowers with diameter 2 μm aggregated on the surface of the substrate, which exhibit step by step growth process. This kind of nanorods and flowers on the top of nanorods are densely and uniformly covered the whole surface of the substrate. Such TiO_2 nanorod flowers provide a large surface area and higher absorption of incident photons, which leads to more photogenerated electron-hole pair, causes higher PEC efficiency [50]. Thus, the well grown nanorod flowers inhibit the electron hole pair recombination rate which is beneficial for improvement in PEC performance. Further increase in reaction time to 8 h the size, length and diameter of nanorods increases (Figure 5d). The sample obtained at this stage shows impulsive aggregated nanorods and nanoparticle which lower the photoelectrochemical performance due to its compactly arranged structure (Figure 5a-5d).

Compositional analysis

An elemental composition of TiO_2 thin films was analyzed by EDS. Figure 6 shows the EDS pattern obtained for representative T_3 sample. There is no trace of any other impurities could be seen within the detection limit of the EDS as presented in Figure 6. The corresponding EDS result indicating that the deposited films mainly consist of Ti and O with an approximate atomic ratio of 1:2 which is in consistent with the stoichiometry of TiO_2. Hence EDS analysis confirms the formation of TiO_2 (Figure 6).

The XPS analysis of TiO_2 thin films was performed to identify the composition and valence state of elements. The survey spectrum of sample T_3 is presented in Figure 7a which shows presence of Ti, O and a small amount of adventitious carbon. The carbon peak is attributed

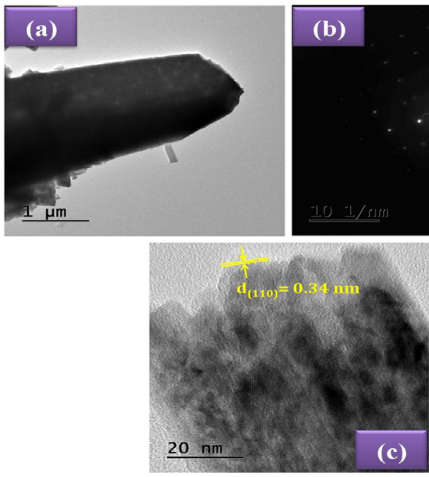

Figure 4: (a) Shows TEM image, (b) SAED pattern and (c) HRTEM image of sample T_3.

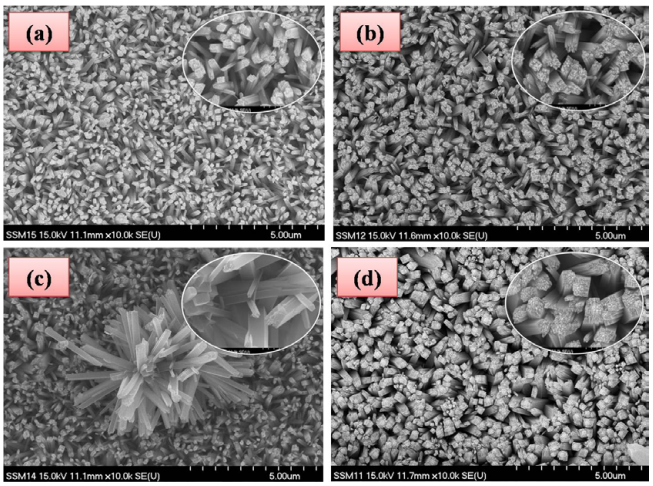

Figure 5: a to d Shows FESEM images of TiO_2 nanostructure samples (T_1–T_4) prepared by varying the reaction time.

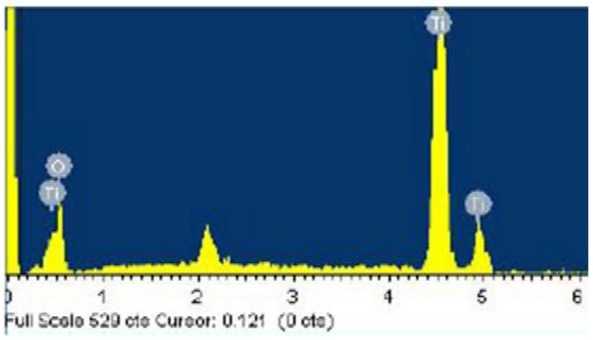

Figure 6: Shows Energy Dispersive X-ray (EDX) spectrum of TiO_2 nanostructure prepared at 6 h reaction times.

to the residual carbon from XPS instrument itself [39]. The peak at binding energy 284.87 eV corresponds to amorphous carbon. Ti 2p spectrum is shown in Figure 7b consists of the distinct Ti /2p1/2 and Ti /2p3/2 signals that are located at 464.4 and 458.6 eV respectively. The spin orbital splitting between these peaks is 5.8 eV which is comparable with that of 5.74 eV reported values, indicates Ti^{4+} oxidation state of titanium in TiO_2 [40]. Both Ti 2p signals are highly symmetric, and no shoulders were observed on the lower energy sides of Ti 2p3/2 signal, which indicate that the rutile TiO_2 nanocrystals are stoichiometric and the concentration of lattice defects is extremely low [41]. The core level spectrum of oxygen is shown in Figure 7c divided into two peaks at binding energy 529.98 and 531.21 eV. The peak located at 529.98 eV attributed to oxygen originating from lattice oxygen while peak at 531.21 eV suggesting the presence of surface hydroxyl groups [42]. The peak at 533.11 eV due to C=O or C-OH group corresponding to the C /1 s species at binding energy 284.87 eV. Thus XPS spectrum confirms the Ti and O species in TiO_2 thin film with rutile phase (Figure 7a-7c).

Photoelectrochemical property

The TiO_2 can absorb large amount of light radiation to form photogenerated electron-hole pair. The photogenerated electrons can transport directly through crystallites and compact layers to the conducting substrates with minimum loss. This photogenerated electrons travel through the external load and completes the circuit by entering back through the counter electrode (Figure 8).

PEC performance of TiO_2 nanorods deposited on FTO substrate is determined by measuring the photocurrent density with a two-electrode configuration under UV (25 W) illumination in 0.1 M NaOH electrolyte. Graphite was served as counter electrode and deposited TiO_2 film as the photoanode. Basically the photocurrent could not be detected unless nanostructured TiO_2 photoanode illumines with UV light, as shown in Figure 8. When the nanostructure photoanode were illuminated under UV light, photovoltage were rises rapidly to a constant value causes shift in the fourth quadrant indicating the generation of electricity, which are typical solar cell characteristics. Following cell configuration was used to record the J-V plots,

Glass - FTO / TiO_2 / NaOH / graphite: The PEC parameters such as fill factor (FF) and PEC efficiency (η%) was calculated by Equation (5) and (6) given below,

$$FF = \frac{Jmax\,Vmax}{Jsc\,Voc} \quad (5)$$

$$\eta\% = \frac{Jsc\,Voc}{Pin} \times FF \times 100 \quad (6)$$

where, '*Vmax*' is maximum voltage, '*Jmax*' is maximum current density, '*Jsc*' is short circuit current density, '*Voc*' is open circuit voltage *and 'Pin'* is intensity of incident light.

The J-V characteristic curves of all the TiO_2 samples are shown in Figure 8. It was found that with increasing reaction time the PEC efficiency increases from 2.9 to 5.1%. The low PEC efficiency for sample T_1 (2 h) is due to immature growth of nanorods. In this case the light

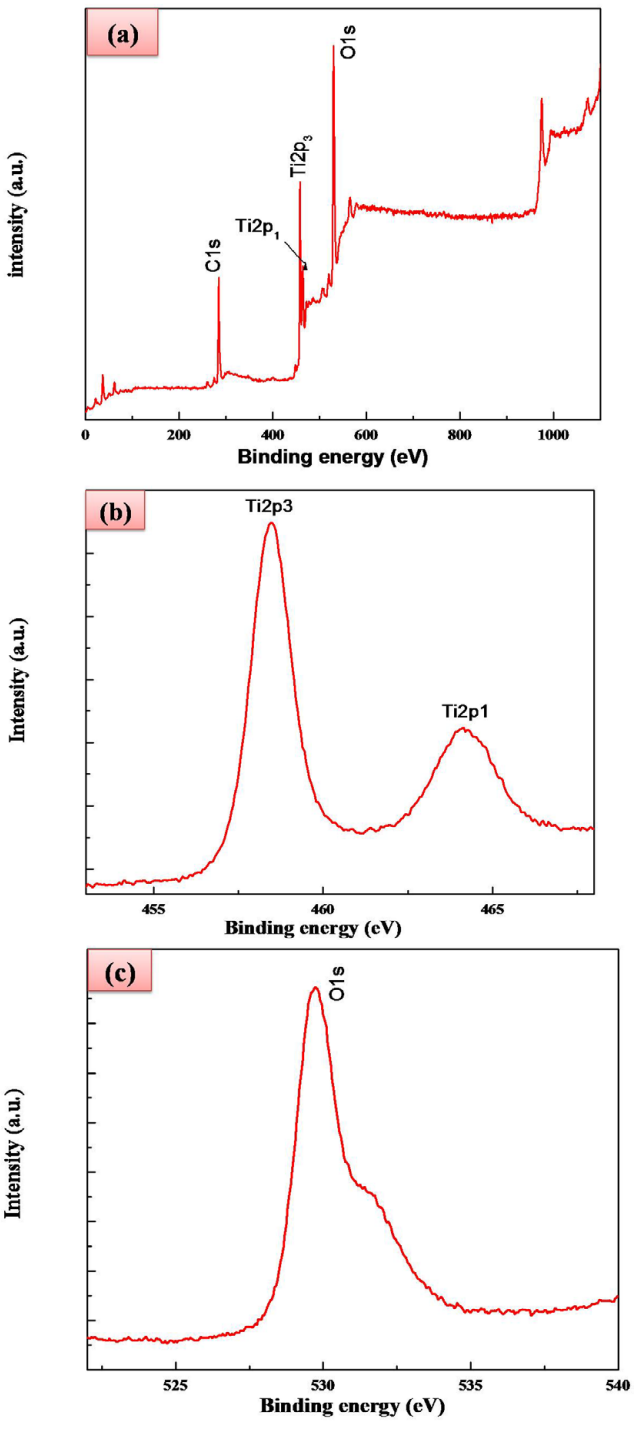

Figure 7: (a) Experimental survey spectrum of TiO_2; (b) Core level spectrum of Ti2p and; (c) Core level spectrum of O1s of TiO_2 thin film.

directly transported through nanorods without scattering results in low PEC efficiency (2.9%). While as the reaction time prolonged to 4 h (sample T_2) it shows 97 μA/cm² photocurrent and 265 mV photovoltage leading to 3.6% PEC efficiency. A sample T_3 (6 h) shows the increased open circuit voltage is 557 mV and short circuit current density is 490 μA/cm² resulting in highest 5.10% PEC efficiency. The increased PEC efficiency contributed by well-developed scattering layers related with 3D TiO_2 nanorod flowers. The advantage of 3D TiO_2 nanorod flowers over 1D nanorods is multireflection, high surface area causes high PEC efficiency [42]. After prolonging the reaction time from 6 h to 8 h there is substantial decrease in current density and results in decrease in photoelectrochemical efficiency up to 3.8%. The decrease in PEC efficiency is due to the compact and aggregated nature of overgrowing nanorods and nanoparticle (Table 1).

These PEC parameters with respect to reaction time are summarized in Table 1. Figure 8 shows plot of conversion efficiency of TiO_2 nanorod flowers synthesized at 160°C for samples deposited at different reaction times. As the deposition time increases the photoconversion efficiency increases up to sample T_3 (5.10%) after that for sample T_4 it again decreases. The enhanced photoelectrochemical performance can be attributed to improved charge-separation by superior charge transportation through crystalline 3D TiO_2 nanorod flowers. This approach may concrete the way to synthesize better TiO_2 electrodes for hybrid solar cells. Transient photoconductivity was studied by exposing the samples with UV-light for 10 s and the response current is measured (Figure 9).

An open circuit voltage-decay measurement is conducted to investigate the recombination kinetics of the nanostructure and is shown in Figure 9. Adopting the technique reported by Zaban et al. open circuit voltage-decay measurements are performed by monitoring the Voc transient during relaxation from an illuminated quasi equilibrium state to the dark equilibrium. The response of these electrodes to UV illumination was very prompt. Hence the TiO_2 nanostructure electrode exhibited superior performance with greater photocurrent generation efficiency.

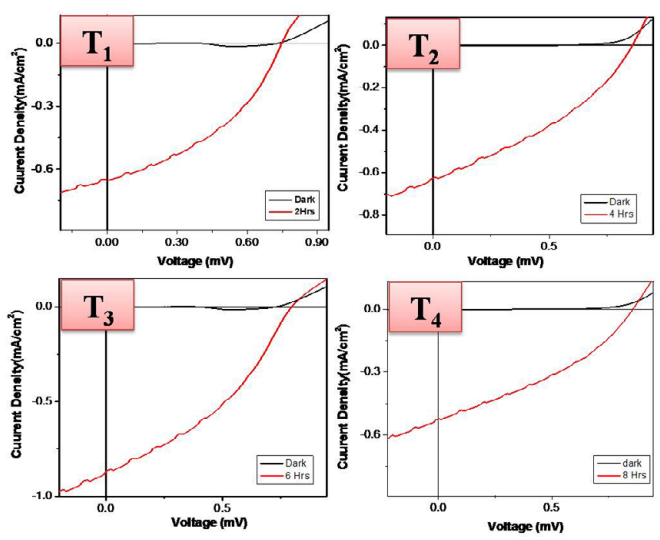

Figure 8: J-V characteristic curve of TiO_2 nanostructure samples (T_1–T_4) prepared by varying the reaction time.

Sample code	V_{oc} (mV)	V_{max} (mV)	J_{sc} (mA/cm²)	J_{max} (mA/cm²)	FF	η %
T_1	834	452	0.528	0.328	0.33	2.9
T_2	893	454	0.685	0.404	0.30	3.6
T_3	794	488	0.872	0.527	0.37	5.1
T_4	747	414	0.654	0.463	0.39	3.8

Table 1: The PEC output parameters of TiO_2 samples.

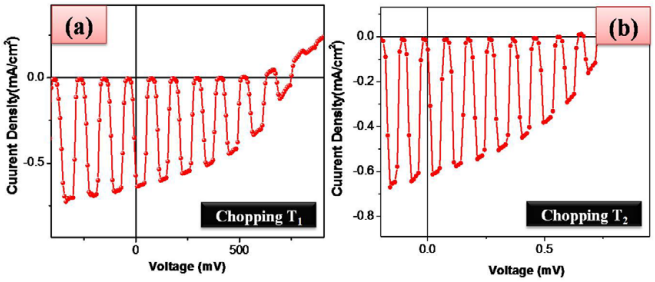

Figure 9: An open circuit voltage-decay measurement of TiO_2 nanostructure sample T_1 and T_4 prepared by varying the reaction time.

Conclusions

We have successfully demonstrated a simple and low cost synthesis method for TiO_2 thin films having well aligned nanorod morphology using single step hydrothermal synthesis. The PEC measurements showed that TiO_2 thin films had maximum photoelectrochemical efficiency of 5.10%. The enhanced PEC performance has been attributed due to stronger light scattering effects, faster electron transportation and electrolyte diffusion in nanorod sample. The results showed that the reaction time plays important role on morphology and PEC performance of TiO_2 samples. Therefore present method is a promising alternative for deposition of TiO_2 thin films with a superior PEC performances therefore it may be allowed for the development of low cost photoelectrochemical devices in future.

Acknowledgments

This research was supported by the Basic Science Research Program through the National Research Foundation of Korea (NRF) funded by the Ministry of Education (NRF-2009-0094055) and outstanding Department of Science and Technology (DST-SERB), New Delhi, under Fast Track Scheme for Young Scientists Major Research Project Funds (Project No. SR/FT/CS-158/2011).

References

1. Santra PK, Kamat PV (2012) Mn-doped quantum dot sensitized solar cells: a strategy to boost efficiency over 5%. J Am Chem Soc 134: 2508-2511.
2. Manthina V, Baena JPC, Liu G, Agrios AG (2012) ZnO–TiO_2 Nanocomposite films for high light harvesting efficiency and fast electron transport in dye sensitized solar cells. J Phys Chem C 116: 23864-23870.
3. Naphade RA, Tathavadekar M, Jog JP, Agarkar S, Ogale S (2014) Plasmonic light harvesting of dye sensitized solar cells by Au-nanoparticle loaded TiO_2 nanofibers. J Mater Chem A 2: 975-984.
4. Guan K (2005) Relationship between photocatalytic activity, hydrophilicity and self-cleaning effect of TiO_2/SiO_2. J Surf Coat Technol 19: 155-160.
5. Linsebigler AL, Lu G, Yates JT (1995) Photocatalysis on TiO_2 surfaces: principles, mechanisms, and selected results. J Chem Rev 95: 735-758.
6. Regan BO, Gratzel M (1991) A low-cost, high-efficiency solar cell based on dye-sensitized colloidal TiO_2 films. Nature 353: 737-740.
7. Li F, He J, Zhou WL, Wiley JB (2003) Synthesis of porous wires from directed assemblies of nanospheres. J Am Chem Soc 125: 16166-16167.

8. Zheng Q, Zhou BX, Bai J, Li LH, Jin ZJ, et al. (2009) Preparation of short, robust and highly ordered TiO_2 nanotube arrays and their applications as electrode. Applied Catalysis B: Environmental 92: 326-332.

9. Wan B, Xing YZ, Jurcakova DH, Wang L (2015) Enhanced performance of a pillared TiO_2 monohybrid as an anode material for fast and reversible lithium storage. J Chem NanoMat: 96-101.

10. Fujishima A, Rao TN, Tryk DA (2000) Titanium dioxide photocatalysis. J Photochem Photobiol C: 1-21.

11. Wang R, Hashimoto K, Fujishima A, Chikuni M, Kojima E, et al. (1997) Light-Induced Amphi-philic Surfaces, Nature 164: 431-432.

12. Lim SH, Luo J, Zhong Z, Ji W, Lin J (2005) Room-temperature hydrogen uptake by TiO_2 nanotubes. Inorg Chem 44: 4124-4126.

13. Wang G, Zhang L, Zhang J (2012) A review of electrode materials for electrochemical supercapacitors. Chem Soc Rev 41: 797-828.

14. Hashimoto K, Irie H, Fujishima A (2005) TiO_2 Photocatalysis: A historical overview and future prospects. Jpn J Appl Phys 44: 8269-8285.

15. Liu D, Xiao P, Zhang Y, Garcia BB, Zhang Q, et al. (2008) TiO_2 Nanotube Arrays Annealed in N_2 for Efficient Lithium-Ion Intercalation. J Phys Chem C 11: 11175-11180.

16. Zhang S, Liu C, Liu X, Zhang H, Liu P, et al. (2012) Nanocrystal Cu_2O-loaded TiO2 nanotube array films as high-performance visible-light bactericidal photocatalyst. Appl Microbiol Biotechnol 96: 1201-1207.

17. Yamaguchi S, Kobayashi H, Narita T, Kanehira K, Sonezaki S, et al. (2010) Novel photodynamic therapy using water-dispersed TiO_2-polyethylene glycol compound: evaluation of antitumor effect on glioma cells and spheroids in vitro. Photochem Photobiol 86: 964-971.

18. Perron H, Vandenborre J, Domain C, Drot R, Roques J, et al. (2007) Combined investigation of water sorption on TiO_2 rutile (110) single crystal face. J Surf Sci 60: 518-527.

19. Li J, Wan W, Zhu F, Li Q, Zhou H, et al. (2012) Nanotube-based hierarchical titanate microspheres: an improved anode structure for Li-ion batteries. Chem Commun (Camb) 48: 389-391.

20. Zhang YX, Li GH, Jin YX, Zhang Y, Zhang J, et al. (2002) Hydrothermal synthesis and photoluminescence of TiO_2 nanowires. J Chem Phys Lett 365: 300-304.

21. Viriya-empikul N, Charinpanitkul T, Sano N, Soottitantawat A, Kikuchi T, et al. (2009) Effect of preparation variables on morphology and anatase-brookite phase transition in sonication assisted hydrothermal reaction for synthesis of titanate nanostructures. J Mater Chem Phys 118: 254-258.

22. Li X, Xiong Y, Li Z, Xie Y (2006) Large-scale fabrication of TiO_2 hierarchical hollow spheres. Inorg Chem 45: 3493-3495.

23. Ho W, Yu JC, Yu JG, Langmuir (2006) Synthesis and characterization of TiO_2 nanorod arrays on glass substrates. Materials Research Bulletin 21: 3486-3490.

24. Yu JG, Su YR, Cheng B (2007) Template-free fabrication and enhanced photocatalytic activity of hierarchical macro-/mesoporous titania. J Adv Funct Mater 17: 1984-1990.

25. Shinde PS, Patil PS, Bhosale PN, Bruger A, Nauer G, et al. (2009) UVA and solar light assisted photoelectrocatalytic degradation of AO7 dye using spray deposited TiO_2 thin films. J Appl Catal B: Environ 89: 288-296.

26. Pradhan SK, Reucroft PJ, Yang F, Dozier A (2003) Growth of TiO_2 nanorods by Metal organic chemical vapor deposition. J Cryst Growth 256: 83-88.

27. Tian ZR, Voigt JA, Liu J, McKenzie B, Xu H (2003) Large oriented arrays and continuous films of TiO(2)-based nanotubes. J Am Chem Soc 125: 12384-12385.

28. Grätzel M (2005) Solar energy conversion by dye-sensitized photovoltaic cells. Inorg Chem 44: 6841-6851.

29. Fan K, Peng T, Chen J, Zhang X, Li R (2013) Low-cost, quasi-solid-state and TCO free highly bendable dye-sensitized cells on paper substrate. J Materials Chemistry 2: 16121-16126.

30. Yang D, Qi L (2000) Egg shell Membrane Templating of Hierarchically Ordered Macroporous Networks Composed of TiO_2 Tubes. J Mater Adv Mater 14: 1543-1546.

31. Haukka S, Lakomaa EL, Root A (1993) An IR and NMR study of the chemisorption of titanium tetrachloride on silica. A J Root Phys Chem 97: 5085-5094.

32. Zhang W, Yang J, Luo Y, Monti S, Carravetta V (2008) Quantum molecular dynamics study of water on TiO_2(110) surface. J Chem Phys 129: 064703.

33. Chu SZ, Wada K, Inoue S, Hishita SI, Kurashima K (2003) Fabrication and structural characteristics of ordered TiO_2-Ru(-RuO_2) nanorods in porous anodic alumina films on ITO/glass substrate. J Phys Chem B 107: 10180-10184.

34. Lau M, Dai L, Bosnick K, Evoy S (2009) Synthesis and characterization of TiOx nanowires using a novel silicon oxide support layer. Nanotechnology 20: 025602.

35. Salari M, Aboutalebi SH, Aghassi A, Wagner P, Mozer AJ, et al. (2015) Disorder engineering of undoped TiO_2 nanotube arrays for highly efficient solar-driven oxygen evolution. Phys Chem Chem Phys 17: 5642-5649.

36. Kim CW, Pal U, Park S, Kim YH, Kim J, et al. (2012) Crystallization Induced porosity control and photocatalytic activity of ordered mesoporous TiO_2. RSC Adv 2: 11969-11975.

37. Abazovi ND, Mirenghi L, Jankovi IA, Bibi N, Soji DV, et al. (2009) Synthesis and Characterization of Rutile TiO(2) Nanopowders Doped with Iron Ions. Nanoscale Res Lett 4: 518-525.

38. Mali SS, Betty CA, Bhosale PN, Patil PS (2011) Hydrothermal synthesis of rutile TiO_2 with hierarchical microspheres and their Characterization. J Cryst Eng Comm 13: 6349-6351.

39. He Z, Liu J, Miao J, Liu B, Thatt T, et al. (2014) A one-pot solvothermal synthesis of hierarchical microspheres with radiallyassembled single crystalline TiO_2 nanorods for high performance dye-sensitized solar cells. J Mater Chem C 2: 1381-1385.

40. Sebo B, Huang N, Liu Y, Tai Q, Liang L, et al. (2013) Dye-sensitized solar cells enhanced by optical absorption, mediated by TiO_2 nanofibers. Acta 112: 458-464.

41. Bisquert J, Santiago FF, Sero IM, Belmonte GG, Gimenez S (2009) Electron lifetime in dye-sensitized solar cells: theory and interpretation of measurements. J Phys Chem C 113: 17278-17290.

42. He Z, Que W, Chen J, He Y, Wang G (2013) Surface chemical analysis of the carbon doped mesoporous TiO_2 photocatalysts after post-thermal treatment: XPS and FTIR characterization. J Phy and Chem 74: 924-928.